



Impacts of Vegetation Losses over Time on Land Surface Temperatures in Borgu Sector of Kainji Lake National Park, Nigeria

A.A. Adeyemi and K.O. Atere

Department of Forest Resources Management,
Faculty of Agriculture,
University of Ilorin, Ilorin, Nigeria

Correspondence: adeyemi.aa@unilorin.edu.ng,

ABSTRACT

The effects of vegetation-changes on land-surface temperature (LST) in Kainji-Lake National Park was evaluated. Hitherto, the possible interaction(s) between land-use/cover, vegetation-index (NDVI) and LST were unknown. This study utilized cloud-free Landsat images within five data-periods (i.e., 1986-1990-1999-2009-2020). The red and near-infrared bands of the images were processed using ArcGIS for NDVI (bands 4 and 3 of Landsat 5 and 7, and bands 5 and 4 of Landsat 8 OLI/TC). Emissivity and LST were determined using thermal-bands 6 for Landsat 5 and 7, and 10 for Landsat 8. Data were analyzed using descriptive statistics and Pearson-correlation. The results revealed that LST increased from $28.46\pm 3.01^{\circ}\text{C}$ (1986) to $34.13\pm 2.07^{\circ}\text{C}$ (2020). However, highest mean-temperature ($41.35\pm 1.16^{\circ}\text{C}$) was in 1999, with the lowest ($28.46\pm 3.01^{\circ}\text{C}$) in 1986. Area with highest temperature had NDVI of 0.120 ± 0.071 , while the NDVI of the area with lowest temperature was 0.436 ± 0.062 . Thus, there were inverse-correlations between NDVI and LST ($r = -0.934, -0.931, -0.992, -0.942$ and -0.972) for 1986, 1990, 1999, 2009 and 2020, respectively. With the decrease of NDVI (vegetation cover), the LST were found to increase. Therefore, there is need to discourage forest-conversions, as losses in vegetation-covers were consequent upon intense anthropogenic-activities such as overgrazing, illegal-logging, fuel-wood exploitation and mining.

Keywords: Forest-conversion - land-surface temperature - land-use/land cover changes.

INTRODUCTION

The world is currently experiencing an unanticipated wave of environmental changes. Abiodun *et al.* (2011) noted that heat waves occur once the maximum temperature is greater than 35°C for 3 days, or more consecutively. Pertinent, therefore, among other requirements, is the assemblage of long-term, consistent and comprehensive data series for climate change research to monitor and offer useful advice on the best approach to environmental manipulation or modifications (Ajibade 2013). An increase in temperature tends to increase the capacity of the atmosphere to hold water and thus, precipitation may increase. However, its effect on climate is spatio-temporal, being controlled by local or regional factors such as topography, vegetation and wind velocity. Hence, both increase and decrease in precipitation rate is envisaged (Panwar and Chakrapani 2013) with rise in temperature.

According to Cernusak *et al.* (2013), combination of high temperature, high irradiance and high vapour pressure deficit can lead to pronounced midday depressions of stomata conductance and CO_2 uptake in tropical forest tree leaves at the upper-canopy. The unique location of the country, traversing three climatic zones and seven ecological zones, makes Nigeria even more vulnerable to the impacts of changing climatic and environmental externalities (Abiodun *et al.* 2011). Despite these events, few studies have concentrated on evaluating the effect of vegetation modification or clearance on changing land surface temperature in most natural forest. Specifically, Kainji Lake National Park has



not been assessed against this background. More so, there is little documentation on reliable data from weather stations in most cases. In the same vein, study of sorts using remote sensing in the study area, are very rare. Thus, the main objective of this study is to assess the effects of variations in vegetation cover on land surface temperature changes.

It is important to explore how local and national climates may already be changing using the most-widely used climate change indicators. This will enable policymakers, environmental managers and authorities at local and national levels to design appropriate and effective mitigation and adaptation mechanisms (Amadi and Udo 2015). This kind of information provides baseline data for developing a long-term strategy of investments to diversify the economy away from climate-sensitive sectors, and strengthening institutional capacity to respond effectively to climate change.

According to Effat *et al.* (2016), land surface temperature is the detection of surface temperature by considering the emissivity of vegetation and emissivity of soils. This can be achieved by analyzing the thermal infrared band of satellite sensors, especially of the Landsat. This is one of the best observations of Land surface temperature to determine the temperature distribution as well as the change in local or global scale, used in climate and climate change models in particular (Himayah *et al.* 2019). Land surface temperature calculated from remote sensing data, is used in many areas including hydrology, agriculture, climate change, urban planning, forestry, among others (Anbazhagan and Paramasivam 2016). Thermal infrared remote sensing provides a unique method for obtaining LST information at the regional and global scales since most of the energy detected by the sensor in this spectral region is directly emitted by the land surface (Jimenez-Munoz and Sobrino 2008).

Adoption of a meaningful approach would help to improve the accuracy of weather forecasting for extended periods. It would also help in studying the factors that determine the statistical properties of the general atmospheric circulation, which would lead to a better understanding of the physical basis of climate. This can be achieved by capitalizing on the availability of high resolution and repetitive coverage of remote sensing techniques (Ojo 2011, Jakub *et al.* 2015). Therefore, this study intends to bridge this gap by implementing algorithms for processing satellite images to analyze changes in temperature of Borgu Sector of the Kainji Lake National Park.

MATERIALS AND METHODS

The Study Area

The Borgu Sector of the Kainji Lake National Park lies between Borgu and Baruten Local Government areas of Niger and Kwara States, on latitudes 9°34'30"N and 10°16'27"N, and longitude 3°34'30"E and 4°37'30"E (Figure 1). It covers an area of about 392,900 ha. The area is bordered to the east by Kainji Lake and in the west by the Republic of Benin. The mean annual rainfall is 1200 mm with a temperature of 30°C and relative humidity of 53%. The amount of rainfall increases to the south-east, from Borgu towards Niger valley. This is due to the leeward nature of the park, being east of Yoruba hills. The number of rainy days averages about 200 in a year. The wet season starts around mid-April and ends early November, giving about seven months of wet season, while the dry season lasts five months, from late November to early April (Bako *et al.* 2015).

The vegetation of the area lies within the Northern Guinea Savannah, and dominated by tree species such as *Azelia africana*, *Isorberlinia tomentosa*, *Burkea africana*, *Isorberlinia doka*, *Crossopteryx ferbrifuga*, *Anogeissus leicarpus*, *Khaya senegalensis*, *Terminalia avicennioides*, *Butryospermum paradoxum*, *Terminalia macroptera*,



Retarium microcarpum, *Diospyros mespiliformis* and *Maytenus senegalensis*. Prominent shrubs include *Piliostigma thonningii* and *Anona senegalensis*. The herb

layer is dominated by *Andropogon gayanus*, *Andropogon tectorum* and *Hyparrhenia sp.* as well as woody forbs such as *Cochlospermum tinctorium*.

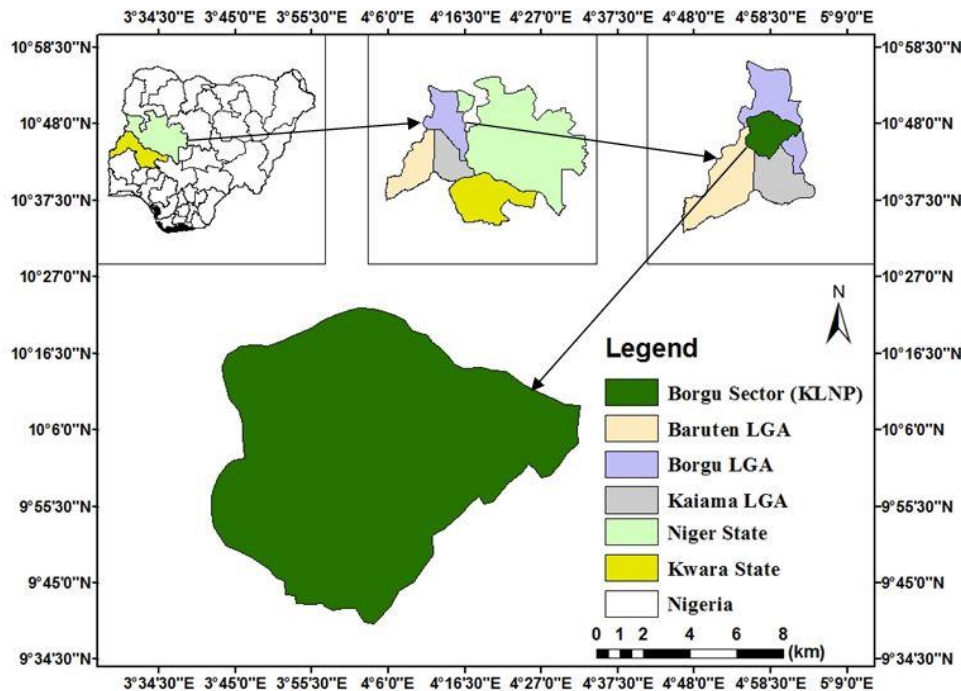


Figure 1: Map of Borgu Sector of Kainji Lake National Park

Remote Sensing Image Data

Remote sensing data for detecting land surface temperature are obtained from the thermal bands, which are the sixth band of Landsat TM and ETM, and 10th and 11th bands for Landsat OLI/TC. To maintain the consistency of data radiation characteristics as well as investigating the detailed thermal structure of land surface more effectively, Landsat images of 1986, 1990, 1999, 2009 and 2020 were chosen as the data sources used for further processing. Landsat TM, ETM+, and OLI/TC scenes covering the study area were selected for the analyses. The images were carefully sourced to eliminate all atmospheric noises such as cloud cover and image scan lines of the years 1986, 1990, 2009 and 2020. All images were acquired from United State Geological

Survey (USGS), which were preprocessed to eliminate radiometric and geometrical distortions.

Image Processing

Different processes for analyzing the Landsat images were used, including derivation of NDVI, retrieval of LST for each image (i.e., radiance, brightness temperature and emissivity). All image processing and analysis were done in ArcGIS 10.5. Thermal bands 6₁ and 6₂ were used for LST extractions from Landsat TM and ETM+, while bands 10 and 11 were used in Landsat 8 OLI/TC for the extractions. Estimation of LST includes radiometric calibration and conversion of digital number (DN), and normalized difference vegetation index analysis, as presented in Figure 2.

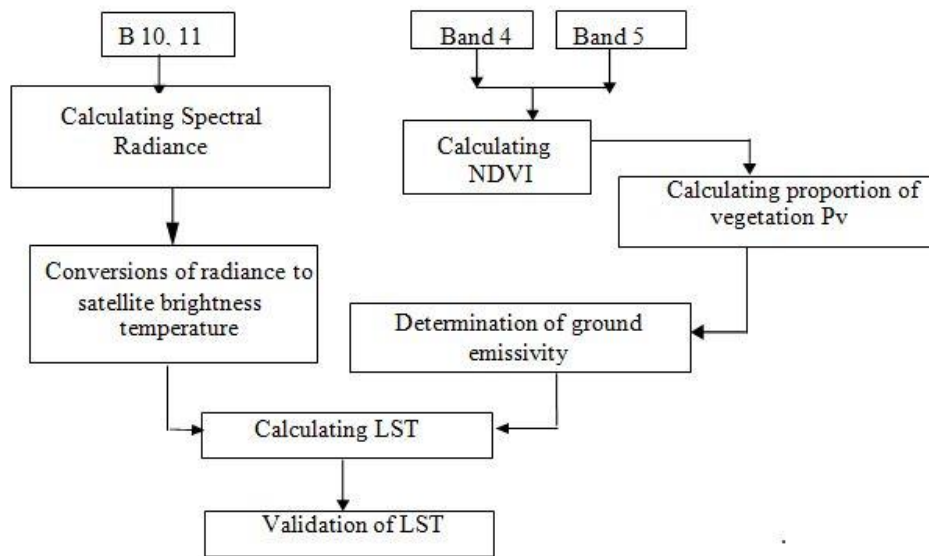


Figure 2: Flow chart for LST and NDVI analyses

Conversion of Digital Number (DN) to Spectral Radiance (Lλ)

Digital number (DN) of bands in Landsat data were converted to spectral radiance in Landsat 5 and 7, as follows:

$$L_{\lambda} = \frac{(L_{max\lambda} - L_{min\lambda})}{(QCAL_{max} - QCAL_{min})} \times (QCAL - QCAL_{min}) + L_{min\lambda} \dots (1)$$

Where:

- Lλ = spectral radiance at the sensor's aperture in watts/m².sr.μm²;
- QCAL = quantized calibrated pixel value in DN;
- Lminλ = spectral radiance scaled to QCALmin in watts/m².sr. μm²;
- Lmaxλ = spectral radiance scaled to QCALmax in watts/m².sr. μm²;
- QCALminλ = minimum quantized calibrated pixel value;
- QCALmax = maximum quantized calibrated pixel value.

While the derivation of spectral radiance for Landsat 8 was determined using:

$$L_{\lambda} = M_L \times QCAL + A_L \dots \dots \dots (2)$$

Where:

- M_L = band-specific multiplicative rescaling factor from the metadata;
- A_L = band-specific additive rescaling;
- QCAL = quantized calibrated pixel value in DN.

Conversion of Spectral Radiance to Brightness Temperature in Kelvin

To convert the spectral radiance values to brightness temperature (in kelvin), the surface brightness temperature of the study area was computed, as follows:

$$BT = K_2 / \ln (1 + K_1 / L_{\lambda} \dots \dots \dots (3)$$

Where:

- BT = brightness temperature of the study area, which equals T_k;
- K₁/K₂ = default pre-launch constants;
- Lλ = radiance of thermal band.

Conversion of Temperature in Kelvin to Celsius

The final apparent surface temperature in Celsius (°C) was computed as:

$$T_c = T_k - 273.15 \dots \dots \dots (4)$$

Where:

- T_c = temperature in Celsius (°C);
- T_k = temperature in Kelvin (K).

Normalized Difference Vegetation Index

Normalized difference vegetation index (NDVI) is a measure of the amount and vigour of vegetation at the surface (Sundara *et al.* 2012). The NDVI is the vegetation index of a pixel. It has been used in a wide variety of studies including those on global vegetation, crop estimation and vegetation



growth, land cover and climate (Benkouider *et al.* 2013). It is expressed as:

$$NDVI = \frac{NIR - RED}{NIR + RED} \dots \dots \dots (5)$$

Where:

- NIR = reflectance in the near-infrared band;
- RED = reflectance in the visible red band.

Normalized difference vegetation index analyzes the percentage variation of vegetal cover in the area showing different vegetation properties. Thus, NDVI has a threshold of -1 to 1.

Surface Emission Rate Determination

Surface emissivity has a considerable effect on the accuracy of LST extraction and the important sources of error. Emissivity was estimated as:

$$E = 0.004P_v + 0.986 \dots \dots \dots (6)$$

Where:

- P_v = proportional vegetation, as is estimated as:

$$P_v = \sqrt{\frac{NDVI - NDVI_{min}}{NDVI_{max} - NDVI_{min}}} \dots \dots \dots (7)$$

Land Surface Temperature

The average atmospheric temperature (LST) was obtained as follows:

$$LST = \frac{BT}{1} + W \times \frac{BT}{P} \times \ln E \dots \dots \dots (8)$$

Where:

- P = planks constant;
- W = wavelength of the emitted radiance as corresponding to the used thermal bands;
- BT = brightness temperature;
- E = emissivity.

Land-use and Land-over Classification

Unsupervised (Iso-cluster) classification technique was adopted to determine the land-use/land-cover (LULC) classes. Field data were collected by obtaining the geographic coordinate values of the different land-cover characteristics of the study site using a hand-held GPS receiver. The vector data were then overlaid on the pre-classified Landsat 8 OLI/TC. In addition, topographic map along with the classified image-data and GPS receiver were used to find the location of the

ground-control points (GCPs) in the field during ground truthing. Thereafter, re-classifications were done to delineate the exact land-use types and their corresponding area coverage in the area. In determining the LULC, land-use/land-cover layers of the selected dates were overlaid in the GIS environment, as done by Adeyemi and Adeleke (2020), Adeyemi and Ibrahim (2020), Adeyemi and Oyeleye (2021). Change analysis was then performed by intersecting the different multi-temporal image layers (for the selected dates: 1986, 1990, 1999, 2009 and 2020). A contingency matrix of change was then developed using appropriate statistics.

LULC Classification Accuracy Assessment

The accuracy for each class was estimated and the accuracy statistics were done based on Rwanda and Ndambuki (2017), as adopted by Adeyemi and Adeleke (2020), Adeyemi and Ibrahim (2020), Adeyemi and Ayinde (2022), as follows:

$$P = \frac{\sum_{i=1}^k n_{ii}}{n} \times 100 \dots \dots \dots (9)$$

Where:

- n_{ii} = number of correct points;
- n = total number of ground control points;
- P = overall accuracy, expressed in percentage.

Sensitivity

$$= \frac{a}{a + b} \text{ (equivalent to Producer's Accuracy) } \dots (10)$$

$$\text{Specificity} = \frac{d}{b + d} \dots \dots \dots (11)$$

$$\text{Commission error} = 1 - \text{Specificity} \dots \dots \dots (12)$$

$$\text{Omission error} = 1 - \text{Sensitivity} \dots \dots \dots (13)$$

Positive Predictive Power

$$= \frac{a}{a + b} \text{ (Equivalent to User's accuracy) } \dots \dots (14)$$

Positive Predictive Power

$$= \frac{d}{c + d} \dots \dots \dots (15)$$

Where:

- a = number of times a classification agreed with the observed value;
- b = number of times a point was classified as X when it was observed to not be X;



c = number of times a point was not classified as X when it was observed to be X;

d = number of times a point was not classified as X when it was not observed to be X.

Total points (accurately classified) = $n = (a + b + c + d)$

The Khat statistics produced by Kappa analysis was computed as:

$$K = \frac{N \sum_{i=1}^r x_{ii} - \sum_{i=1}^r (x_{ij} + Xx_{+1})}{N^2 - \sum_{i=1}^r (x_{ij} + Xx_{+1})} \dots \dots \dots (16)$$

Where:

r = number of rows and columns in error matrix;

N = total number of observations (pixels);

X_{ii} = observation in row i and column i ;

X_{ij} = marginal total of row i ;

X_{+i} = marginal total of column i .

A Kappa coefficient equal to 1 means perfect agreement between the observed and the expected, whereas a value close to zero means that the agreement is no better than would be expected by chance.

RESULTS

Land-use and Land-cover Changes in the Study Area

Table 1 presents the description of the four land-use/land-cover (LULC) types distinguished in the study area. These include forest, savannah, water body/swamp and bareland/built-up area.

Table 2 presents spatial distribution of land-use and land-cover in the study area. In 1986, grassland covered 205,142 ha (49%) followed by forest with about 118,337 ha (28%). Water body/swamp covered about 21,990 (5%), while the bareland/built-up area occupied 75,560 ha (18%) of the area. In 2020, savannah increased to 294,332 (ha), constituting about 70% of the total area, reclaiming parts of forest and water body/swamp. Thus, forest and water body/swamp declined to 76,804 ha (10%) and 5,725 ha (1.4%), respectively (Figure 3).

Table 1: Description of land covers

| LULC | Description |
|------------------------|--|
| Forest | Dense vegetation consisting of trees and other flora. |
| Savannah | Areas dominated by grasses with some scattered shrubs and trees in very sparse arrangements. |
| Water body/swamp | Areas covered by rivers, streams, drains, lakes, ponds and swamps. |
| Bareland/built-up area | Areas with no vegetation and/or with building structures and other infrastructures. |

Table 2: Spatial extent of LULC between 1986 and 2020

| LULC | 1986 | | 1990 | | 1999 | | 2009 | | 2020 | |
|-------|---------|------|---------|------|---------|------|---------|------|---------|------|
| | Area | % |
| F | 118,337 | 28.1 | 124,592 | 29.6 | 93,363 | 22.2 | 27,431 | 6.5 | 76,804 | 18.2 |
| SV | 205,142 | 48.7 | 173,410 | 41.2 | 309,012 | 73.4 | 173,547 | 41.2 | 294,332 | 69.9 |
| WB/S | 21,990 | 5.2 | 8,636 | 2.1 | 5,372 | 1.3 | 624 | 0.1 | 5,725 | 1.4 |
| BB | 75,560 | 17.9 | 114,393 | 27.2 | 13,282 | 3.2 | 219,427 | 52.1 | 44,168 | 10.5 |
| Total | 421,030 | 100 | 421,030 | 100 | 421,030 | 100 | 421,030 | 100 | 421,030 | 100 |

N.B.: F - forest; SV - savannah; WB/S - water body/swamp; BB - bareland/built-up area

Table 3: Changes in LULC between 1986 and 2020

| LULC class | 1986 | 1990 | 1999 | 2009 | 2020 | 1986-2020 | |
|------------|-----------|-----------|-----------|-----------|-----------|--------------------|------------|
| | Area (ha) | Δ LULC (ha) | % Δ |
| F | 118,337 | 124,592 | 93,363 | 27,431 | 76,804 | -41,533 | -35.1 |
| SV | 205,142 | 173,410 | 309,012 | 173,547 | 294,332 | 89,190 | 43.5 |
| WB/S | 21,990 | 8,636 | 5,372 | 624 | 5,725 | -16,265 | -74.0 |
| BB | 75,560 | 114,393 | 13,282 | 219,427 | 44,168 | -31,392 | -41.5 |
| Total | 421,030 | 421,030 | 421,030 | 421,030 | 421,030 | - | - |

N.B.: F - forest; SV - savannah; WB/S - water body/swamp; BB - bareland/built-up area

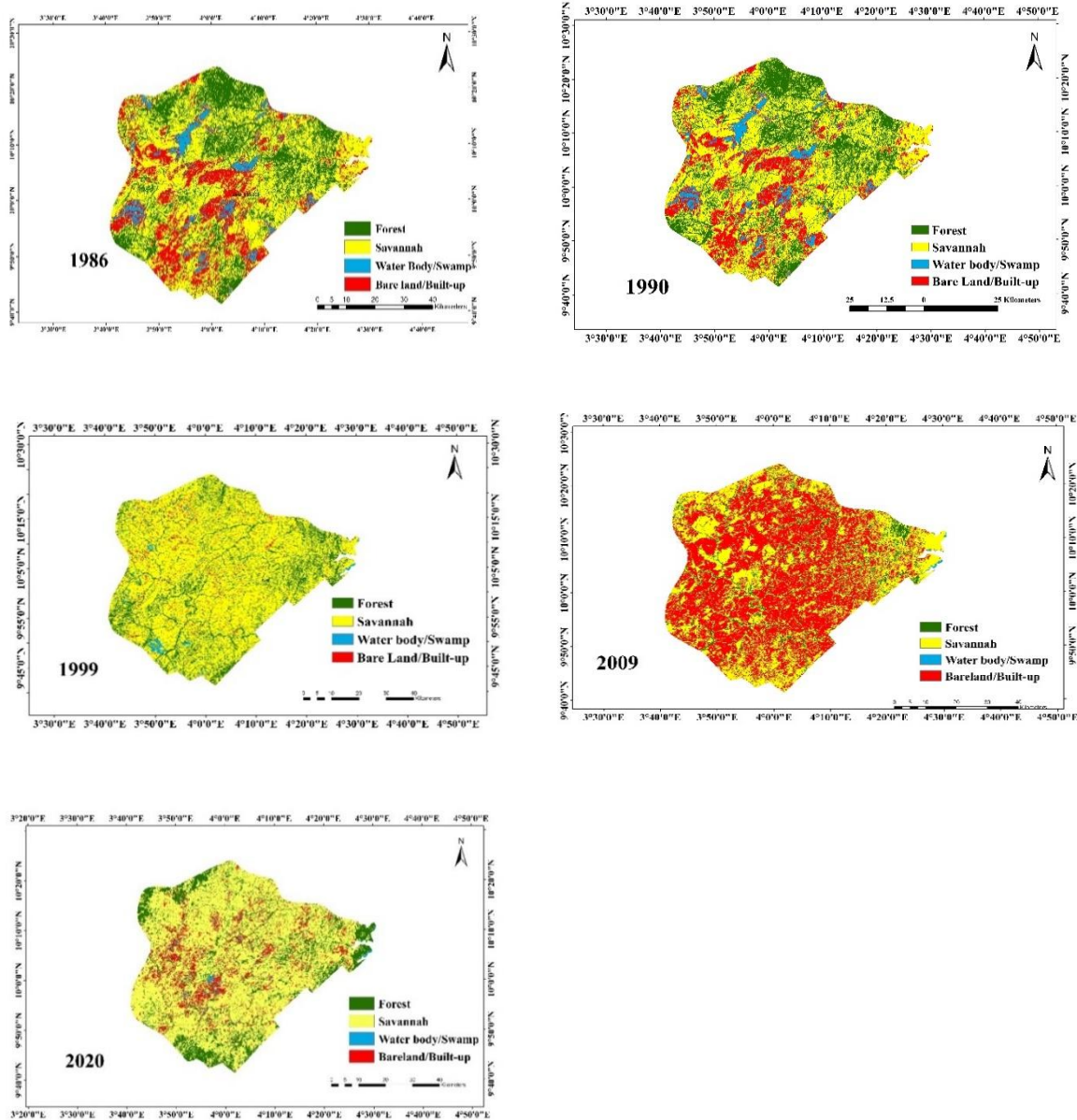


Figure 3: LULC maps of Borgu Sector between 1986 and 2020

Table 3 presents the trend of changes in LULC in the area between 1986 and 2020. Forest area and water body/swamp shrank by 35.1% and 74.0%, respectively. Savannah, however increased by 43.5% of its original extent in 1986, while 42% of the barelands/built-up areas were reclaimed by savannah in 2020.

The confusion matrix for LULC classification accuracy assessment is shown

in Table 4. The correct values for each class are arranged diagonally (20, 58, 16 and 24). Table 5 presents the result of LULC classification accuracy assessment. The overall accuracy was 88.7%, producer's accuracies ranged between 0.8 and 0.83, while user's accuracies were between 0.87 and 0.857. The overall Kappa's coefficient obtained for the classification was 0.84, implying that the classification accuracy was substantial.



Table 4: Confusion matrix

| LULC class | Forest | Savannah | Water Body/Swamp | Bareland/built-up area | Total |
|------------------------|--------|----------|------------------|------------------------|-------|
| Forest | 20 | 0 | 1 | 2 | 23 |
| Savannah | 2 | 58 | 1 | 0 | 61 |
| Water body/swamp | 2 | 0 | 16 | 3 | 21 |
| Bareland/built-up area | 1 | 1 | 2 | 24 | 28 |
| Column total | 25 | 59 | 20 | 29 | 133 |

Table 5: Classification accuracy assessment results

| LULC class | UA | PA | Sensitivity | Specificity | CE | OE |
|------------------------|------|------|-------------|-------------|-------|-------|
| Forest | 0.87 | 0.80 | 0.80 | 0.97 | 0.028 | 0.200 |
| Savannah | 0.95 | 0.98 | 0.98 | 0.96 | 0.041 | 0.017 |
| Water body/swamp | 0.76 | 0.80 | 0.80 | 0.96 | 0.044 | 0.200 |
| Bareland/built-up area | 0.86 | 0.83 | 0.838 | 0.96 | 0.039 | 0.172 |

UA - user's accuracy; PA - producer's accuracy; CE - commission error; OE - omission error

Normalized Difference Vegetation Index (NDVI) of Borgu Sector between 1986 and 2020

Table 6 and Figure 4 present the NDVI results for Borgu Sector of Kainji Lake National Park. The maximum NDVI (0.436 ± 0.062) was in 1990, which shows the appearance of denser vegetation and canopy in that year compared to other periods, however, this does not imply more vegetated areas in comparison to other years studied, but only shows that vegetation was thickest in some areas during that period. The lowest value (-0.036 ± 0.061) was in 2009, indicating presence of less-dense vegetation.

Land Surface Temperatures (LST) of Borgu Sector between 1986 and 2020

Table 7 and Figure 5 present LST of Borgu Sector in the five periods studied. The results

revealed that high temperature areas correspond to built-up areas, bareland and dried or silted water body/swamp whereas the cooler areas were forests and then grassland. Temperature was highest in 1999 with a mean of $41.35 \pm 1.16^\circ\text{C}$, while 1986 had the least mean temperature of $28.46^\circ\text{C} \pm 3.01$. However, in 1990, 2009 and 2020 the mean temperatures were $34.93^\circ\text{C} \pm 2.90$, $32.05^\circ\text{C} \pm 2.92$ and $34.13^\circ\text{C} \pm 2.07 \pm 2.07$, respectively.

Table 8 presents correlations (r) between NDVI and LST for the five periods. There was inverse relationship between NDVI and LST, implying that as NDVI value drops, temperature begins to rise. In other words, areas with low NDVI values tend to have high temperature, and vice-versa (Figure 6).

Table 6: NDVI values for Borgu Sector between 1986 and 2020

| Year | NDVI values | | | | | | Mean \pm SD |
|------|-------------|--------|--------|--------|-------|-------|--------------------|
| 1986 | -0.364 | 0.017 | 0.071 | 0.128 | 0.178 | 0.546 | 0.120 ± 0.071 |
| 1990 | -0.756 | -0.042 | 0.006 | 0.061 | 0.128 | 0.787 | 0.436 ± 0.062 |
| 1999 | -0.538 | -0.183 | 0.072 | 0.172 | 0.235 | 0.527 | 0.194 ± 0.059 |
| 2009 | -0.434 | -0.212 | -0.077 | -0.021 | 0.041 | 0.283 | -0.036 ± 0.061 |
| 2020 | -0.049 | -0.003 | 0.006 | 0.015 | 0.027 | 0.076 | 0.010 ± 0.010 |

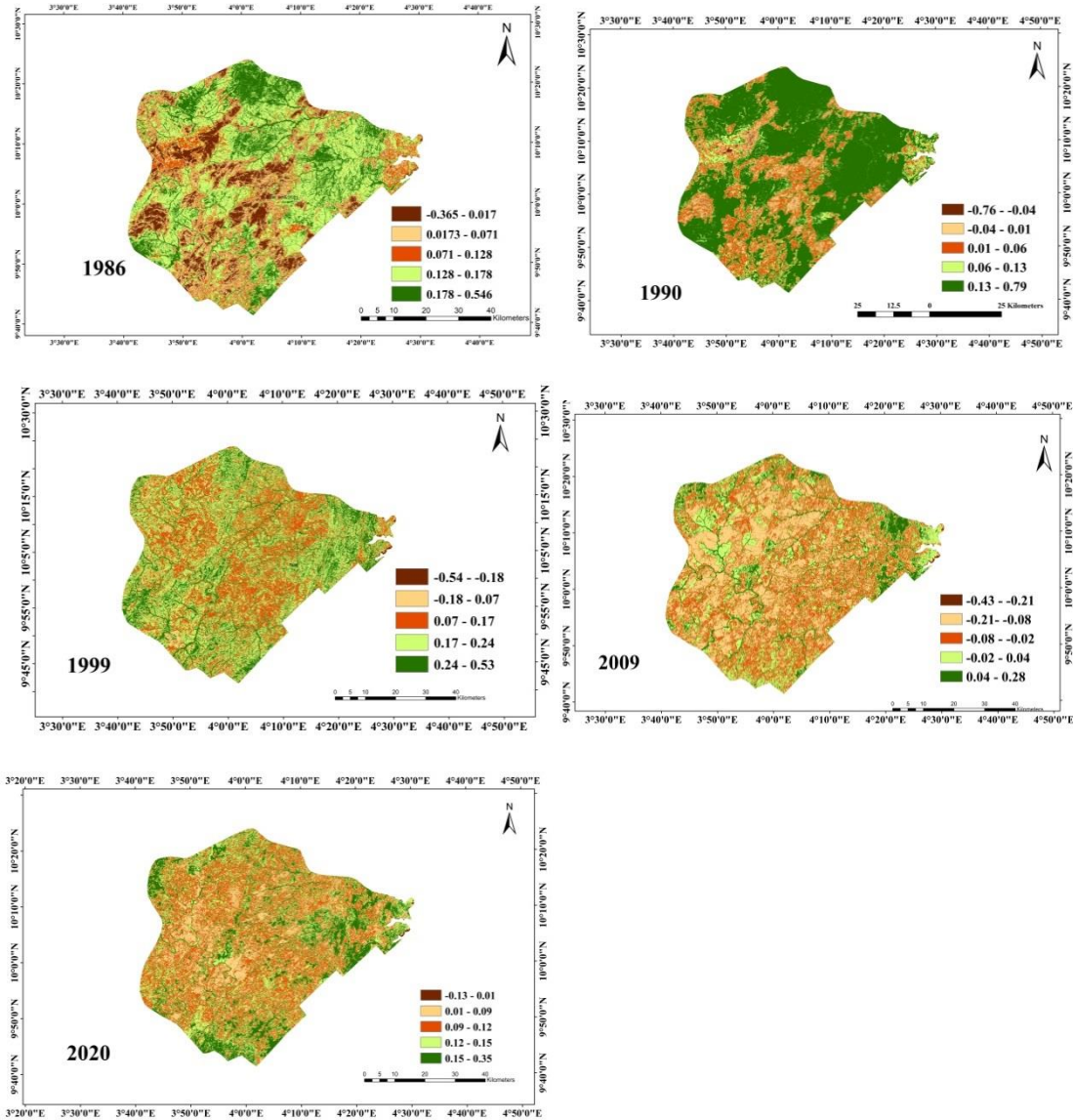


Figure 4: NDVI maps of Borgu Sector between 1986 and 2020.

Table 7: Spatial distribution of LST in Borgu Sector between 1986 and 2020

| Year | LST (°C) | | | | | | |
|------|----------|--------|----------|-------|-------|-------|--------------|
| | Min. | Forest | Savannah | WB/S | BB | Max. | Mean ± SD |
| 1986 | 21.06 | 27.90 | 31.14 | 37.61 | 49.49 | 66.94 | 28.46 ± 3.01 |
| 1990 | 24.92 | 31.74 | 34.65 | 37.01 | 47.24 | 64.45 | 34.93 ± 2.90 |
| 1999 | 22.86 | 27.84 | 28.80 | 30.24 | 33.12 | 41.35 | 41.35 ± 1.16 |
| 2009 | 21.82 | 29.65 | 32.53 | 34.80 | 45.51 | 74.36 | 32.05 ± 2.92 |
| 2020 | 22.51 | 31.17 | 33.04 | 34.68 | 36.32 | 52.35 | 34.13 ± 2.07 |

SD - standard deviation; WB/S - water body/swamp; BB - bareland/built-up area

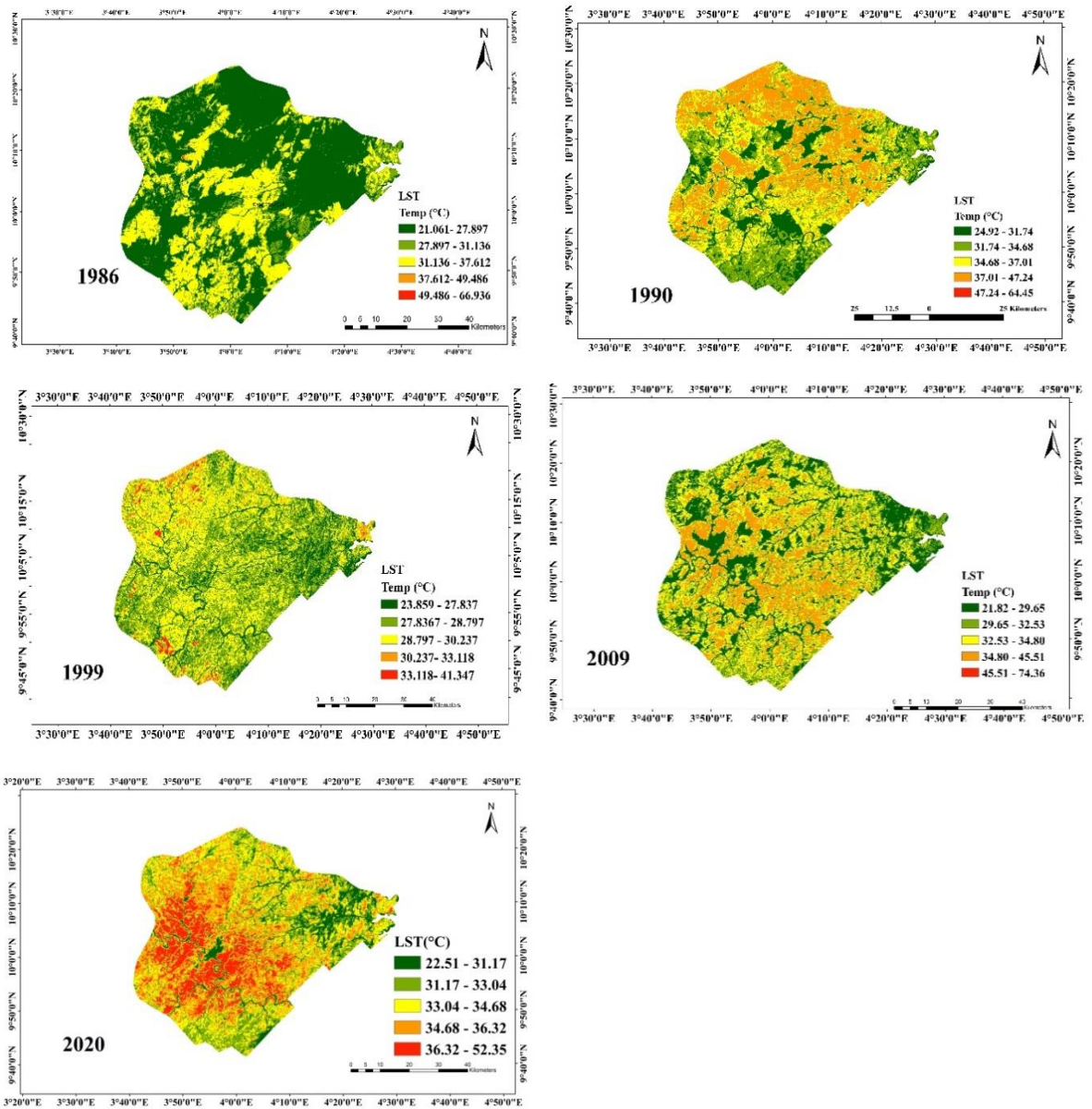
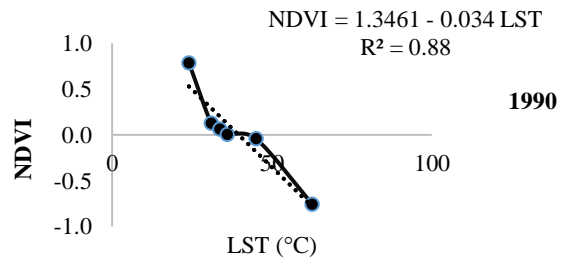
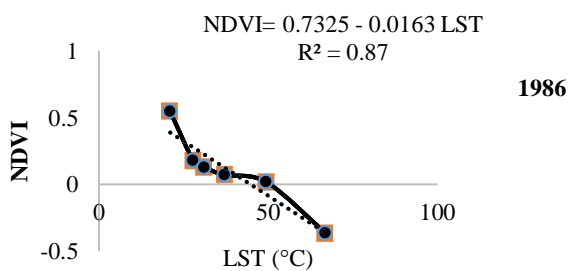


Figure 5: Land surface temperature maps of Borgu Sector between 1986 and 2020

Table 8: Correlation between NDVI and LST

| Year | r |
|------|--------|
| 1986 | -0.934 |
| 1990 | -0.931 |
| 1999 | -0.992 |
| 2009 | -0.942 |
| 2020 | -0.958 |



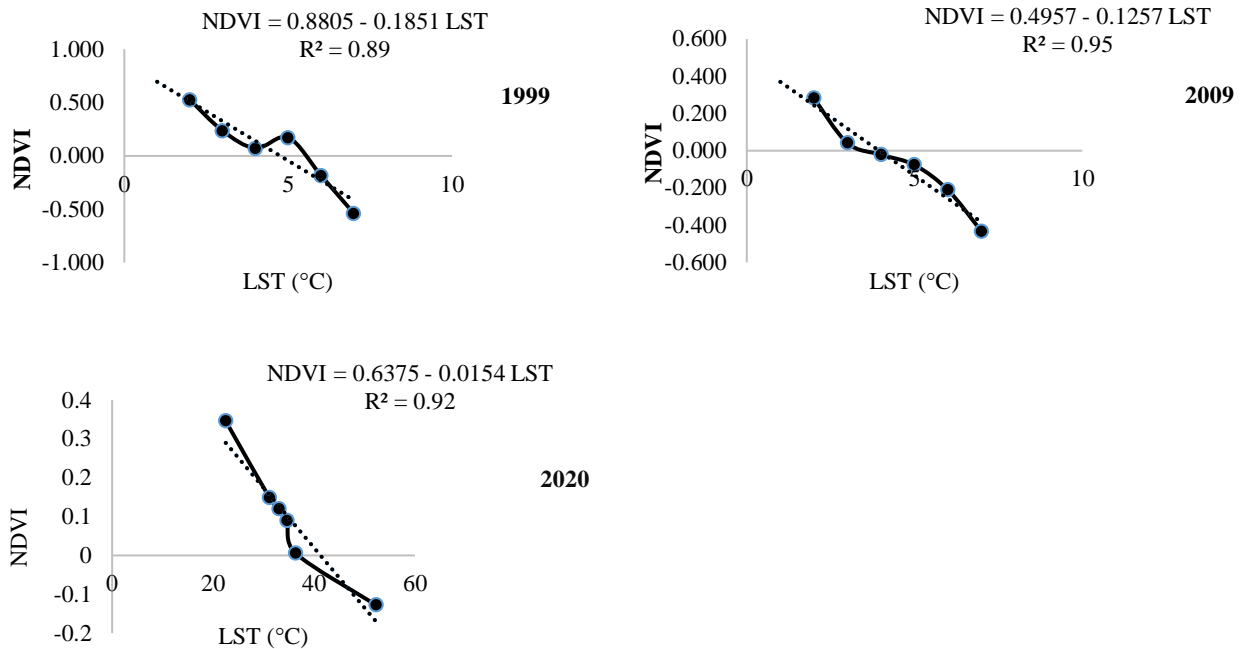


Figure 6: Relationships between NDVI and LST in Borgu Sector from 1986 to 2020.

DISCUSSION

The results showed that areas with more green vegetation were lower in average land surface temperature, when compared to areas with little or no vegetation, as in bare land/built-up areas within the study area. This is similar to the observation of Himayah *et al.* (2019), who noted that when the LST value is high, the value of green vegetation is low, and if the LST value is low then the green vegetation value would be high. The bareland/built-up areas in the study area occurred as a result of occasional anthropogenic disturbances in forms of forest clearances, illegal-logging, overgrazing by cattle herders and mining. The sensitivity of vegetation indices to variations in land surface temperature observed in this study agrees with the work of Mohammed *et al.* (2019), who noted how sensitive vegetation indices were to changes in land surface temperature. A similar observation was made by Yuan and Bauer (2007) that, areas with high NDVI are usually found to have lower land surface temperature and vice versa. Mallick *et al.* (2008) also examined the relationship between the NDVI and the LST using

Landsat 7 ETM+ data and found significantly strong relationship between the two variables. The land-cover category of dense vegetation (forest) and highly-dense built-up areas showed the highest ($r = -0.752$) and the lowest ($r = -0.394$) inverse relationships. This is, however, contrary to the report by Sun and Kafatos (2007), who observed positive correlation between LST and NDVI in temperate region during winter, perhaps due to the accumulation of snow and cold weather.

We found that seasonal streams and swamps without water, or those that were silted-up due to vegetation clearances, or forest degradation, through overgrazing, illegal logging and mining, were higher in temperature compared to streams or swamps in better conditions with water and less-silted. This corroborates the finding of Joshi and Bhatt (2012), who reported that areas with vegetation and water body had lower temperatures than built-up areas or areas without these two components. Essentially, land surface temperatures were significantly influenced by land-use practices or land cover-types, as areas with lower vegetation covers were higher in temperature and



hotter. Increases in temperatures were also found in areas with lesser water, which resulted either from reduced precipitation, or siltation due to vegetation losses. This is in line with the observations of Spracklen *et al.* (2012), who noted that persistent large-scale land-use changes and forest conversion have great potentials to alter or influence rainfall patterns.

According to Salih *et al.* (2012), alteration in rainfall patterns may affect the vegetation of a given area, just as it is also possible that there could be reduced rainfall in forested areas as resulting from deforestation occurring somewhere else. Hasler *et al.* (2009) observed that reduction in rainfall as a result of deforestation can lead to reduction in evapotranspiration, up to 80% reduction in annual rainfall in deforested areas. Abbas *et al.* (2010) stated that change of land-use/land-cover significantly aggravates surface runoff, soil erosion, land degradation, sedimentation, siltation, drought, migration, desertification, loss of biodiversity, and ultimately, decrease in land productivity.

Moreover, during the period investigated, changes in land-use and cover-types were becoming more intense, and mainly linked to anthropogenic pressure in quest for human livelihood supports. Anthropogenic activities including overgrazing by cattle herders, illegal-logging and mining were observed to be the major drivers of vegetation losses in the area, as identified in the course of fieldwork and ground-truthing, all of which were unauthorized since the area is under protection. This is in line with Meduna *et al.* (2009), who observed that illegal activities were the main drivers of gross forest disappearances, especially in the tropics.

CONCLUSION AND RECOMMENDATIONS

The study has shown that there were land-cover/use changes in Borgu Sector of the Kainji Lake National Park between 1986 and

2020. It is established that LST increases with a decrease in vegetation cover. There was a strong indication that anthropogenic activities (forest conversion, overgrazing and mining) significantly influenced the variations in LST. Thus, LST inversely correlated with NDVI. This may have negative implications for forest/soil biodiversity. The capability of the area to sequester carbon may also be affected by losses in vegetation. Therefore, it is recommended that further losses in vegetation be checked. One of the means to maintain biodiversity conservation is to sustainably manage the area while educating the surrounding communities on better approaches to conservation. Remote sensing was adequate for evaluating relationship between vegetation cover (NDVI) and variation in LST. The overall classification accuracy was very good, suggesting a reasonable-measure of reliability of the classification scheme used.

REFERENCES

- Abbas, I.I., Muazu, K.M. & Ukoje, J.A. 2010. Mapping land use-land cover and change detection in Kafur local government, Katsina, Nigeria (1995-2008) using remote sensing and GIS. *Research Journal of Environmental and Earth Sciences* 2(1): 6-12.
- Abiodun, B.J., Salami, A.T. & Tadross, M. 2011. Climate change scenarios for Nigeria: Understanding biophysical impacts. Climate systems analysis group, Cape Town, for Building Nigeria's Response to Climate Change (BNRCC) project, Ibadan, Nigeria. Nigerian Environmental Study/Action Team NEST 11pp.
- Adeyemi, A.A. & Adeleke, S.O. 2020. Assessment of Land-cover Changes and Carbon Sequestration Potentials of Trees Species in J4 Section of Omo Forest Reserve, Ogun State, Nigeria. *Ife Journal of Science* 22(1): 137-152.



- Adeyemi, A.A. & Ayinde, M.O. 2022. Evaluation of Land-Use and Land-Cover Changes in Oba Hills Forest Reserve, Osun State, Nigeria. *Forestist* 72(2): 137-148.
- Ajibade, I.M. (2013): Climate change and human rights: A case study of vulnerability and adaptation in coastal communities in Lagos, Nigeria. Unpublished Ph.D. Thesis, University of Western Ontario, London, ON, Canada 159pp.
- Adeyemi, A.A. & Ibrahim, T.M. 2020. Spatiotemporal Analysis of Land-use and Land cover Changes in Kainji Lake National Park. *Forestist* 70(2): 105-115.
- Adeyemi, A.A. & Oyeleye, H.A. 2021. Evaluation of Land-use and Land-cover Changes Cum Forest Degradation in Shasha Forest Reserve, Osun State, Nigeria Using Remote Sensing. *Tanzania Journal of Forestry and Nature Conservation* 90(2): 27-40.
- Amadi, S.O. & Udo, S.O. 2015. Climate change in contemporary Nigeria: An empirical analysis of trends, impacts, challenges, and coping strategies. *Journal of Applied Physics* 7(2): 1-15.
- Anbzhagan, S. & Paramasivam, C.R. 2016. Statistical Correlation between Land Surface Temperature (LST) and Vegetation Index (NDVI) using Multi-Temporal Landsat TM Data. *International Journal of Advanced Earth Science and Engineering* 5(1): 333-346.
- Bako, M.M., Musa, J., Suleman, M.M., Kuta, G.I. & Eno. G. 2015. An assessment of vegetal cover transition in the Zugurma sector of Kainji Lake National Park. *Nigeria Journal of Environment and Earth Science* 5: 925-948.
- Benkouider, F., Abdellaoui, A., Hamami, L. & Elaihar, M. 2013. Spatio-temporal analysis of vegetation by vegetation indices from multi-dates satellite images: Application to a semi-arid area in Algeria. *Energy Procedia* 36: 667-675.
- Cernusak, L.A., Winter, K., Dalling, J.W., Holtum, J.A., Jaramillo, C., Körner, C., Leakey, A.D. & Norby, R.J. 2013. Tropical forest responses to increasing atmospheric CO₂: Current knowledge and opportunities for future research. *Functional Plant Biology* 40: 531-550.
- Effat, H.A. & Hassan, O.A.K. 2014. Change Detection of Urban Heat Islands and Some Related Parameters Using Multi-Temporal Landsat Images: A Case Study for Cairo City, Egypt. *Urban Climate* 10: 171-188.
- Hasler, N., Werth, D. & Avissar, W. 2009. Effects of tropical deforestation on global hydro climate: A multimodel ensemble analysis. *Journal of Climate* 22(5): 1124-1141.
- Himayah, S., Ismail, A., Nandi, A., Ridwana, R., Arrasyid, R., Affriani, A.R. & Ihsan, M. 2019. Correlation between Land Surface Temperature and Vegetation Greenness using Multi-temporal Images. *IOP Conf. Series: Earth and Environmental Science* 286. doi:10.1088/1755-1315/286/1/012043.
- Jakub, F. & Mayer, B. 2015. A three-dimensional parallel radiative transfer model for atmospheric heating rates for use in cloud resolving models: The TenStream solver. *Journal of Quantitative Spectroscopy and Radiative Transfer* 163: 63-71.
- Jimenez-Munoz, J.C. & Sobrino, J.A. 2008. Split-Window Coefficients for Land Surface Temperature Retrieval from Low-Resolution Thermal Infrared Sensors. *IEEE Geoscience Remote Sensing Letters* 5: 806-809.
- Joshi, P.J. & Bhatt, J. 2012. Estimating temporal land surface temperature using remote sensing: A study of



- Vadodara urban area, Gujarat. *International Journal of Geology, Earth and Environmental Sciences* 2(1): 123-130.
- Meduna, A.J., Ogunjimi, A.A. & Onadeko, S.A. 2009. Biodiversity conservation problems and their implications on ecotourism in Kainji Lake National Park, Nigeria. *Journal of Sustainable Development in Africa* 10(4): 59-73.
- Mohammed, S.O., Gajere, E.N., Eguaroje, E.O., Shaba, H., Ogbole, J.O., Mangut, Y.S., Onyeuwaoma, N.D. & Kolawole, I.S. 2013. Spatio-temporal analysis of the National Parks in Nigeria using geographic information system. *Ife Journal of Science* 15: 159-165.
- Ojo, M.O., Olanusi, O.B. & Akinnubi, R.T. 2011: Application of meteorology and weather prediction in the sustainable environmental quality in Nigeria. *Journal of Environmental Issues and Agriculture* 3: 100-105.
- Rwanga, S.S. & Ndambuki, J.M. 2017. Accuracy assessment of land use/land cover classification using remote sensing and GIS. *International Journal of Geosciences* 8: 611-622.
- Salih, A., Körnich, I. & Tjernström, M. 2012. Climate impact of deforestation over South Sudan in a regional climate model. *International Journal of Climatology* 10: 1002-1026.
- Spracklen, D., Arnold, S. & Taylor, C. 2012. Observations of increased tropical rainfall preceded by air passage over forests. *Nature* 489: 282-288.
- Sun, D. & Kafatos, M. 2007. Note on the NDVI-LST relationship and the use of temperature-related drought indices over the North America. *Geophysical Research Letters* 34(24): 128-138.
- Sundara-Kumar, K., Udaya-Bhaskar, P. & Padmakumari, K. 2012. Estimation of Land Surface Temperature to Study Urban Heat Island Effect Using Landsat ETM+ Image. *International Journal of Engineering, Science and Technology* 4(2): 771-778.
- Yuan, F. & Bauer, M. 2007. Comparison of impervious surface area and normalized difference vegetation index as indicators of surface urban heat island effects in Landsat imagery. *Remote Sensing of Environment* 106(3): 375-386.